Optics & Laser Technology 42 (2010) 1209–1217

Contents lists available at ScienceDirect

Optics & Laser Technology

journal homepage: www.elsevier.com/locate/optlastec

Numerical analysis and optimization of a dual-concentric-core photonic crystal fiber for broadband dispersion compensation

M. Alirameza ni *, Sh.Mohammad Nejad

Nanoptronics Research Center, Department of Electrical Engineering, Iran University of Science and Technology, Tehran, 16846-13114, Iran

ARTICLE INFO

Article history:
Received 24 October 2009
Received in revised form
10 March 2010
Accepted 28 March 2010
Available online 18 April 2010

Keywords:
Dual-concentric-core photonic crystal fiber
Dispersion compensation
Loss

ABSTRACT

In this article, a novel dual-concentric-core photonic crystal fiber (DC-PCF) for dispersion compensation is presented. The proposed DC-PCF has relatively high negative dispersion over a wide wavelength range, which covers E, S, C, L and U telecommunication wavelength bands. The validity of the proposed design is carried out by employing a 2-D finite difference frequency domain method (FDFD) with perfectly matched layers (PML). By using the numerical method, the dispersion profile of the DC-PCF is optimized in terms of three air-hole diameters to achieve desirable negative dispersion. The influence of the location of ring-core, the number of air-hole rings on dispersion and loss characteristics are also studied.

1. Introduction

Recently, the traffic over transmission lines has increased rapidly. Wavelength division multiplexing (WDM) technique higher bit-rate transmissions of more than 40 Gb/s have widely been adopted to handle increasing data capacity [1,2]. The transmission impairment caused by dispersion in a single mode fiber (SMF) is severe for such high-bit-rate transmissions. This has made dispersion compensation techniques essential.

Dispersion compensating fibers (DCFs) are perhaps the most widely used platforms for compensating the dispersion accumulated over a transmission link. This improves the transmission length without the need of using electronic regeneration of signals [3].

On the other hand, index-guiding photonic crystal fibers (PCFs), also known as holey fibers, have particularly attracted considerable attention from the optical scientific community. Usually PCFs are all pure silica fibers with a regular array of air-holes running along the length of the fiber acting as the cladding. A defect in the periodical structure acts as a core. One of the appealing properties of PCFs is the fact that they can possess dispersion properties significantly different from those of the conventional optical fibers, because their artificially periodic cladding consisting of micrometer-sized air-holes allows the flexible tailoring of the dispersion curves [4–6]. Additionally, the precise control of the geometrical parameters can provide high negative dispersion in PCFs.

Various DCFs that were optimized to compensate for the dispersion in a single band, e.g., the S-band (1460–1530 nm), C-band (1530–1565 nm), L-band (1565–1625 nm), and U-band (1625–1675 nm), have been reported [7,8]. It has also been reported that combining two or more dispersion compensation fibers can realize broadband compensation from the C-band to the L-band [9]. However, it is difficult for the DCF to compensate for dispersion over lower band, i.e. the E-band (1360–1460 nm). This is because the material dispersion has a strong effect. It is therefore difficult to control the dispersion over all the telecommunication bands.

In recent years, several designs of dispersion compensating PCFs have been reported. Most of the PCF designs were based on dual-concentric-core refractive index profile. In this type of design, the PCF supports two cores, called central core and ring-core. In the presence of ring-core, if geometrical parameters of PCF are well selected, large negative dispersion can be obtained [10].

The main objective of this article is designing a dual-concentric-core PCF (DC-PCF) to compensate dispersion over a wide wavelength range by varying each air-hole diameter along the radius. This paper is organized as follows. In the next section, the theory of FDFD is described. Sections 3 and 4 focus on the DC-PCF analysis procedure and structure, respectively. Finally, numerical results are discussed in Section 5.

2. Analysis method

Two dimensional finite difference frequency domain (2-D FDFD) is popular and appealing for numerical electromagnetic simulation due to its many merits. The discretization scheme can be derived from the Helmholtz equations [11] or Maxwell's

* Corresponding author.
E-mail addresses: Mohammad_Alirameza ni@ee.iust.ac.ir (M. Alirameza ni), Shahramm@iust.ac.ir (Sh. Mohammad Nejad).

0030-3992/$ - see front matter © 2010 Elsevier Ltd. All rights reserved.
doi:10.1016/j.optlastec.2010.03.012

equations [12] directly. Now we use the direct discretization schemes first described for photonic crystal fibers by Zhu and Brown [12]. Yee's two-dimensional mesh is illustrated in Fig. 1: note that the transverse fields are tangential to the unit cell boundaries, so the continuity conditions are automatically satisfied. After inserting the equivalent nonsplit-field anisotropic PML [13] in the frequency domain, the curl Maxwell equations are expressed as

$$\begin{aligned} jk_0 s\varepsilon_r E &= \nabla \times H \\ -jk_0 s\mu_r H &= \nabla \times E \end{aligned} \tag{1}$$

$$s = \begin{bmatrix} \frac{s_y}{s_x} & & \\ & \frac{s_x}{s_y} & \\ & & s_x s_y \end{bmatrix} \tag{2}$$

where μ_r and ε_r are the relative permittivity and permeability of the medium considered, and $k_0=2\pi/\lambda$ is the wave number in free space. For exp $(-j\omega t)$ convention, which is used in this paper:

$$s_x = 1-\frac{\sigma_x}{j\omega\varepsilon_0},\ s_y = 1-\frac{\sigma_y}{j\omega\varepsilon_0} \tag{3}$$

where σ conductivity the medium considered and ε_0 is permeability in free space.

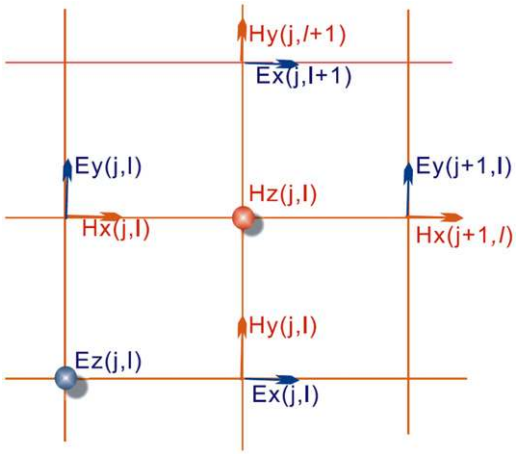

Fig. 1. . Unit cell in Yee's 2D–FDFD mesh.

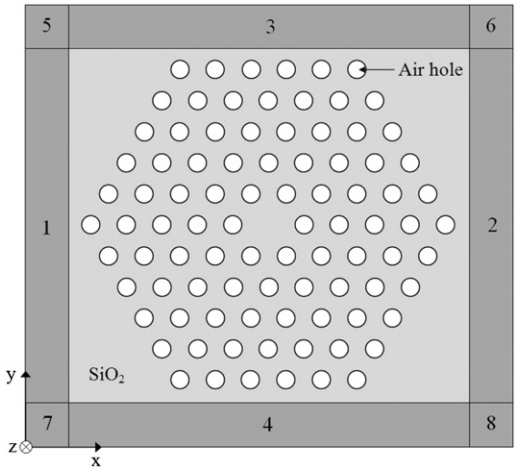

Fig. 2. Calculating model of transverse cross section of photonic crystal fiber surrounded by PMLs.

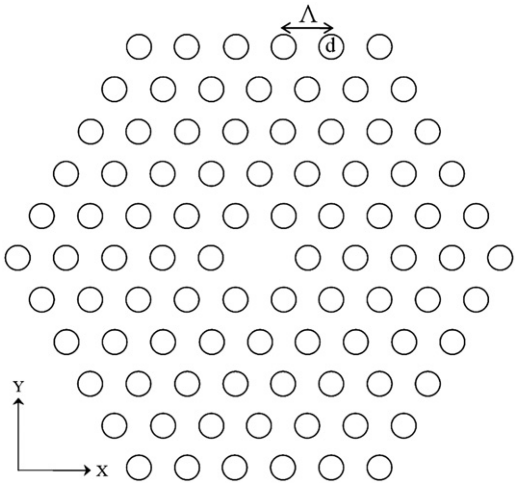

Fig. 3. Cross-sectional view of the test case PCF [14].

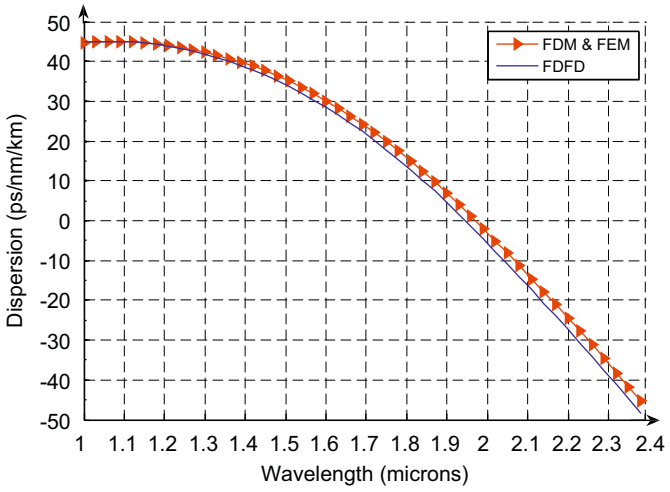

Fig. 4. Dispersion curve of the test case PCF as a function of wavelength by using FDM, FEM and FDFD. $d=1$ μm, $\Lambda=2.3$ μm.

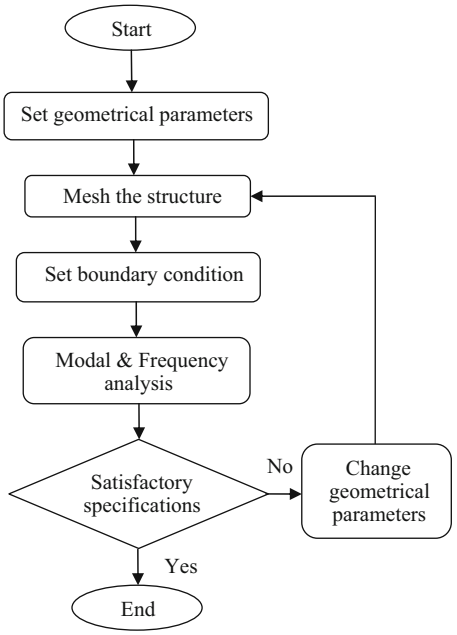

Fig. 5. Design process of the DC-PCF.

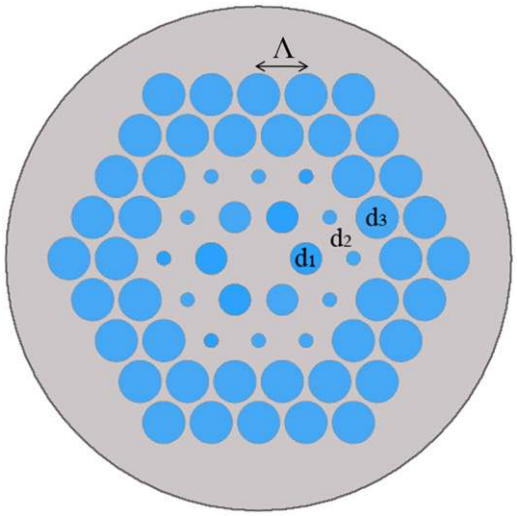

Fig. 6. Cross-sectional view of the DC-PCF.

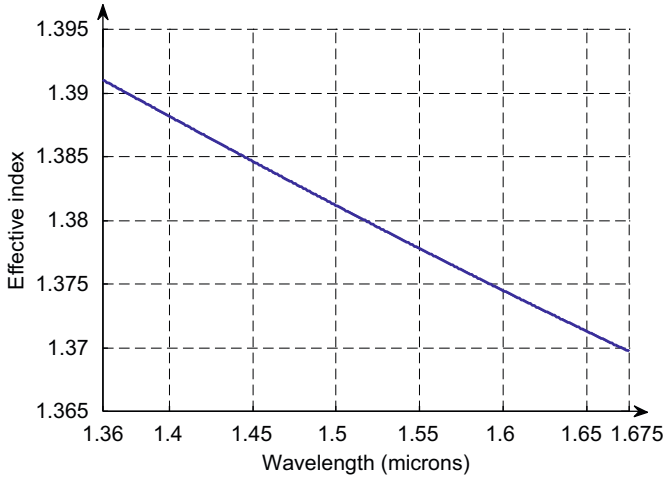

Fig. 7. Effective index curve of the DC-PCF as a function of wavelength. $d_1=1$ μm, $d_2=0.45$ μm, $d_3=1.35$ μm and $\Lambda=1.5$ μm. $n_{silica}=1.44$ and $n_{air}=1$.

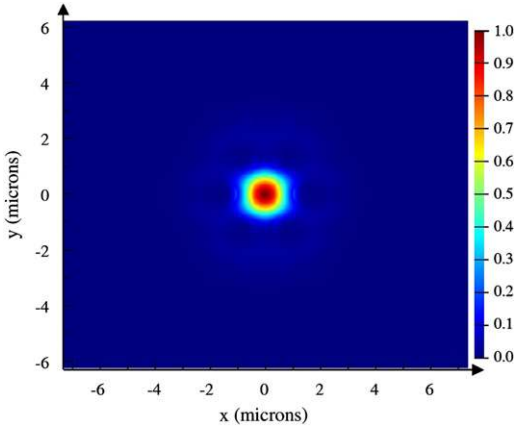

Fig. 8. Transversal field intensity distribution at a wavelength of $\lambda=1550$ nm for the fundamental guiding mode. $d_1=1$ μm, $d_2=0.45$ μm, $d_3=1.35$ μm and $\Lambda=1.5$ μm.

In the compact-2D scheme for waveguides, the z-derivatives are replaced by analytical expressions using (1), and other derivatives are replaced by finite differences in Yee's mesh.

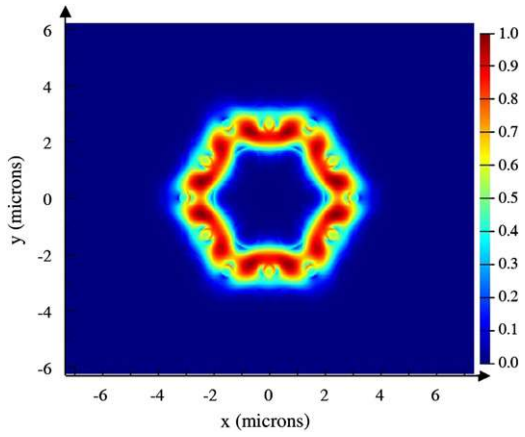

Fig. 9. Transversal field intensity distribution at a wavelength of $\lambda=1550$ nm for the ring-core mode. $d_1=1$ μm, $d_2=0.45$ μm, $d_3=1.35$ μm and $\Lambda=1.5$ μm.

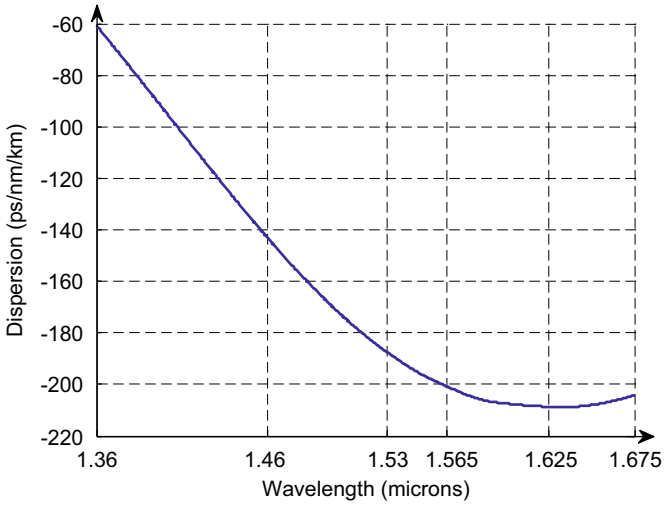

Fig. 10. Dispersion curve of the DC-PCF as a function of wavelength. $d_1=1$ μm, $d_2=0.45$ μm, $d_3=1.35$ μm and $\Lambda=1.5$ μm.

Therefore, the curl (1) can be expressed in matrix form [13]:

$$-jk_0\begin{bmatrix}\frac{S_y}{S_x}\varepsilon_{rx} & & \\ & \frac{S_x}{S_y}\varepsilon_{ry} & \\ & & S_xS_y\varepsilon_{rz}\end{bmatrix}\begin{bmatrix}E_x\\E_y\\E_z\end{bmatrix}=\begin{bmatrix}0 & -j\beta(I) & V_y\\ j\beta(I) & 0 & -V_x\\ -V_y & V_x & 0\end{bmatrix}\begin{bmatrix}H_x\\H_y\\H_z\end{bmatrix} \tag{4a}$$

$$jk_0\begin{bmatrix}\frac{S_y}{S_x}\mu_{rx} & & \\ & \frac{S_x}{S_y}\mu_{ry} & \\ & & S_xS_y\mu_{rz}\end{bmatrix}\begin{bmatrix}H_x\\H_y\\H_z\end{bmatrix}=\begin{bmatrix}0 & -j\beta(I) & U_y\\ j\beta(I) & 0 & -U_x\\ -U_y & U_x & 0\end{bmatrix}\begin{bmatrix}E_x\\E_y\\E_z\end{bmatrix} \tag{4b}$$

where U and V are sparse matrices, which are obtained in the same way as in [13,14] and I is an identity matrix.

Eliminating the longitudinal magnetic and electric fields, the eigenvalue matrix equation in terms of transverse magnetic fields and transverse electric fields can be obtained as

$$\begin{bmatrix}Q_{xx} & Q_{xy}\\ Q_{yx} & Q_{yy}\end{bmatrix}\begin{bmatrix}H_x\\H_y\end{bmatrix}=\beta^2\begin{bmatrix}H_x\\H_y\end{bmatrix} \tag{5a}$$

and

$$\begin{bmatrix} P_{xx} & P_{xy} \\ P_{yx} & P_{yy} \end{bmatrix} \begin{bmatrix} E_x \\ E_y \end{bmatrix} = \beta^2 \begin{bmatrix} E_x \\ E_y \end{bmatrix} \tag{5b}$$

where Q and P are highly sparse coefficient matrices [14]. The order and the nonzero elements in them are reduced and effectively stored in sparse format, so the computation efficiency is improved greatly. The complex propagation constant β and the transversal magnetic or electric field distribution can be solved quickly and accurately by a sparse matrix solver.

Fig. 2 shows the cross section of a PCF surrounded by PML regions 1–8, where x and y are the transverse directions, z is the propagation direction, PML regions 1, 2 and 3, 4 are faced towards x- and y-direction, respectively, and regions 5–8 correspond to the four corners.

For validation of our simulations with the FDFD, simulated results are compared with results of [15,16], which used vector finite difference method (FDM) and finite element method (FEM), respectively. The cross-sectional view of the test case PCF is shown in Fig. 3. Parameters of the PCF are $d=1$ μm, $\Lambda=2.3$ μm, $n_{silica}=1.44$, and $n_{air}=1$. Fig. 4 illustrates the dispersion characteristic of the PCF by using FDM [14], FEM [15], and FDFD. According to Fig. 4, the simulated results by the FDFD are in excellent agreement with the FDM and the FEM simulation.

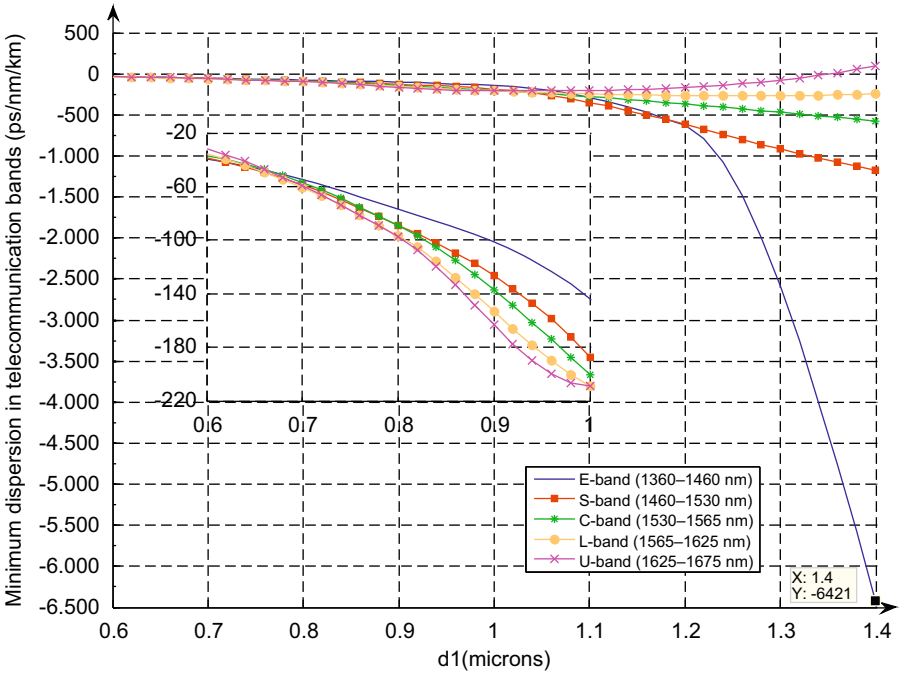

Fig. 11. Minimum dispersion of the DC-PCF in E, S, C, L and U band as a function of d_1. $d_2=0.45$ μm, $d_3=1.35$ μm and $\Lambda=1.5$ μm

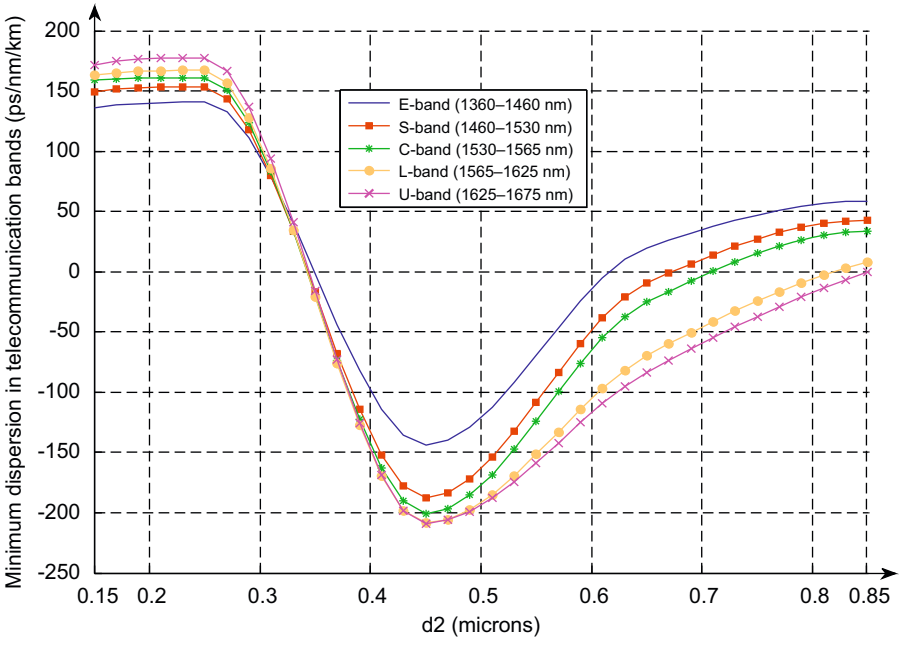

Fig. 12. Minimum dispersion of the DC-PCF in E, S, C, L and U band as a function of d_2. $d_1=1$ μm, $d_3=1.35$ μm and $\Lambda=1.5$ μm.

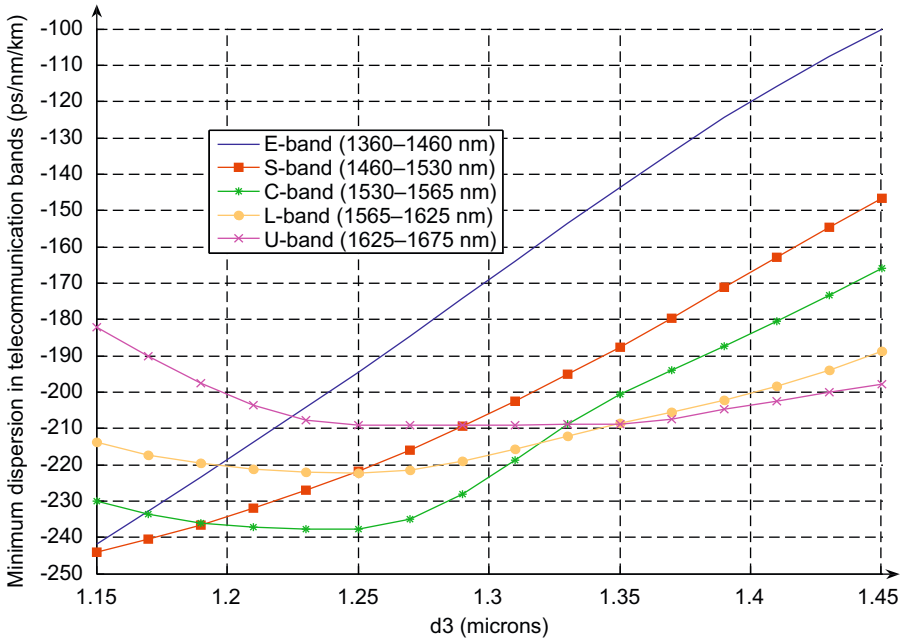

Fig. 13. Minimum dispersion of the DC-PCF in E, S, C, L and U band as a function of d_3. $d_1=1$ μm, $d_2=0.45$ μm and $\Lambda=1.5$ μm.

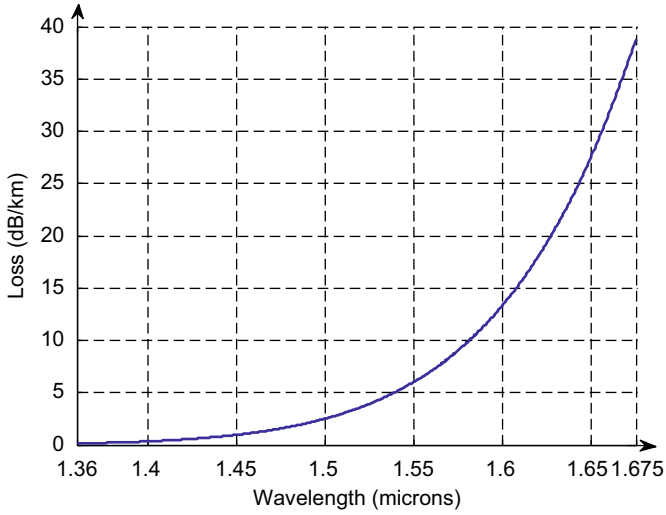

Fig. 14. Loss curve of the DC-PCF as a function of wavelength. $d_1=1$ μm, $d_2=0.45$ μm, $d_3=1.35$ μm and $\Lambda=1.5$ μm.

3. The DC-PCF design and analysis

The design process of a DC-PCF requires the steps shown in Fig. 5. The essential geometric parameters of the DC-PCF configuration are chosen in the first step. These parameters include shape and size of the air-holes, the distance between the nearest air-holes (pitch), the number of air-holes rings and the background material. After that, analysis precision should be determined, and based on the precision, the structure should be meshed. Then with respect to the structure symmetries, the boundary conditions should be set in such a manner that the analysis time becomes minimum.

Mode analysis refers to the calculating propagation constant (β) of the structure modes and evaluation of the guided modes for selecting a well confined mode.

The DC-PCF characteristics of the selected mode, e.g. effective index, dispersion, and loss, are calculated in frequency analysis. It is noteworthy that the desirable specification of DC-PCF designs is ultra-high flattened negative dispersion while the loss characteristic is feasible.

In an index-guiding PCF, the core index is greater than the average index of the cladding because of the presence of air-holes, and the fiber can guide the light by total internal reflection as a standard fiber does. That is, the guided light has an effective index n_{eff} that satisfies the condition

$$n_{co} > n_{eff} = \frac{\beta}{k_0} > n_{FSM} \tag{6}$$

where β is the propagation constant along the fiber axis, k_0 is the wave number in free space, n_{eff} is effective index n_{co} is the core index, and n_{FSM} is the cladding effective index of the FSM. In the case of a PCF made from pure silica, n_{co} is reduced to the index of silica [17].

The dispersion characteristic is obtained by the following equation:

$$D(\lambda) = -\frac{\lambda}{c}\frac{d^2 n_{eff}}{d\lambda^2} \tag{7}$$

where c is the velocity of light in vacuum. When the hole diameter to pitch ratio is very small and the hole pitch is large, the dispersion curve is close to the material dispersion of pure silica. As the air-hole diameter is increased, the influence of waveguide dispersion becomes stronger.

Due to the finite number of air-holes that can be made in the fiber cross section, all the PCF guided modes are leaky. Under this circumstance, the effective index is a complex value and the confinement loss proportionate to imaginary part of β and is calculated by using

$$L_c = 8.686 \times \mathrm{Im}[\beta] \tag{8}$$

4. The DC-PCF geommterical struture

The cross-sectional view of the proposed DC-PCF is presented in Fig. 6. The DC-PCF offers dispersion controllability over a broadband wavelength range by using three different air-hole diameters, such that $d_3 > d_1 > d_2$. Since the designed DC-PCF

consists of a solid core with a regular array of air-holes acting as the cladding, the proposed DC-PCF is a high index core. This type of PCF may be defined as one where the mean cladding refractive index in the long-wavelength limit $k \to 0$ is lower than the core index (in the same limit). Under correct conditions (high airfilling fraction), PBG guidance may also occur in this case, but the TIR-guided modes will be dominant [18].

The air-holes diameters (d_1, d_2 and d_3) are optimized to achieve large negative dispersion, broadband dispersion compensation, and low loss. Geometric parameters of the DC-PCF are $d_1=1$ μm, $d_2=0.45$ μm, $d_3=1.35$ μm. Also, the pitch has been chosen as $\Lambda=1.5$ μm and the refractive index is $n=1.44$ of silica in calculation.

Figs. 7 and 8 show the effective index profile and the mode field distribution of the DC-PCF at a wavelength of 1550 nm. The mode field distribution had its maximum amplitude at the center core region and spread to the second core region. Since the mode field of the DC-PCF is largely inside the inner core, the dispersion

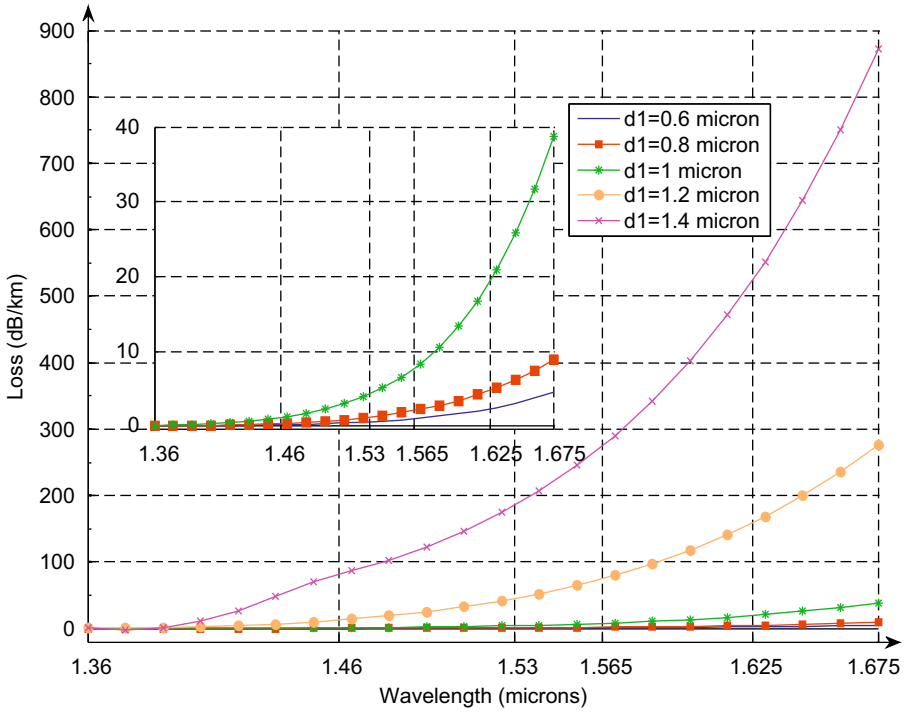

Fig. 15. Loss curve of the DC-PCF as a function of wavelength with different d_1 $d_2=0.45$ μm, $d_3=1.35$ μm and $\Lambda=1.5$ μm.

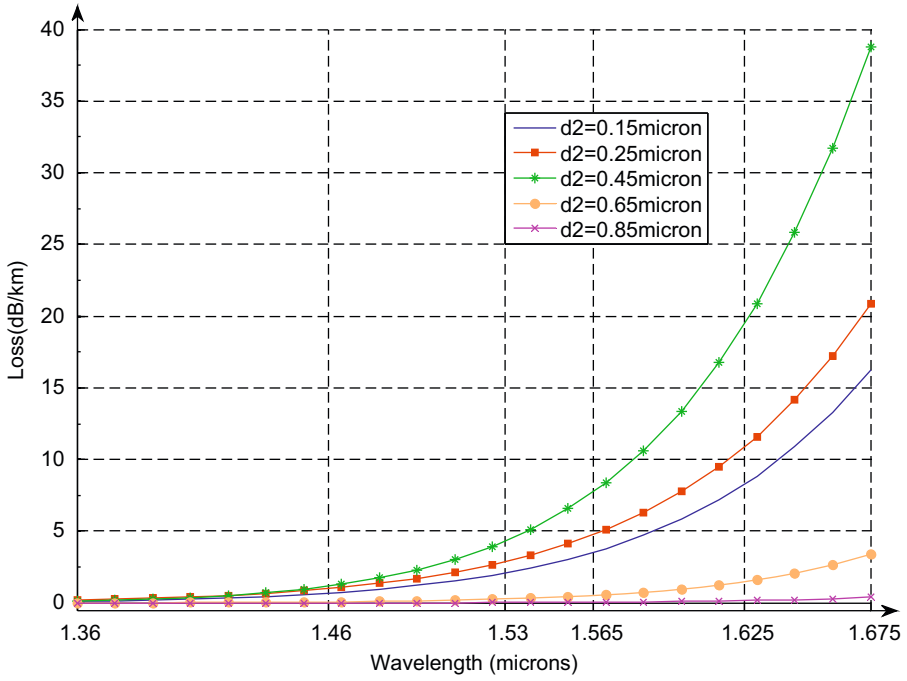

Fig. 16. Loss curve of the DC-PCF as a function of wavelength with different d_2. $d_1=1$ μm, $d_3=1.35$ μm and $\Lambda=1.5$ μm.

characteristic of the DC-PCF is more sensitive to the inner core structure. Furthermore, it can be seen that the fundamental mode is well confined to the core area (see Fig. 8).

Fig. 9 illustrates ring core mode of the DCP-CF. By using (9) effective mode areas of the inner core A_{eff1} and the ring core A_{eff2} are 7.06 and 28.27 μm^2, respectively. Note that it is roughly equal to that of the high nonlinear fiber, and is not too small to be accepted in WDM systems.

$$A_{eff} = \frac{\left(\iint_s |E_t|^2 dx\, dy\right)^2}{\iint_s |E_t|^4 dx\, dy} \tag{9}$$

where E_t is the transverse electric field vector and s denotes the whole fiber cross section.

5. Numerical results

As mentioned above, the proposed DC-PCF employs three different air-hole diameters to produce relatively high negative dispersion in a wide wavelength range. The dispersion curve of the DC-PCF with optimized parameters $d_1=1$ μm, $d_2=0.45$ μm, $d_3=1.35$ μm and $\Lambda=1.5$ μm from the E-band to the L-band is shown in Fig. 10. As it can be seen, the designed DC-PCF has negative dispersion of −143.7 to −61.5 (ps/nm/km) over the E-band. Furthermore, the DC-PCF shows negative dispersion of −187.6 to −143.7 (ps/nm/km), −200.6 to −187.6 (ps/nm/km), −208.7 to −200.6 (ps/nm/km), and −208.8 to −204 over S, C, L, and U bands, respectively.

Figs. 11–13 demonstrate the minimum dispersion of the DC-PCF in E, S, C, L, and U bands with altering the hole diameters of the inner three rings: d_1, d_2, and d_3, respectively.

With respect to Figs. 11–13, the highest negative dispersion occurred in the E-band for DC-PCF with $d_1=1.4$ μm, $d_2=0.45$ μm, $d_3=1.35$ μm and $\Lambda=1.5$ μm that achieves ultra-high negative dispersion of −6421 (ps/nm/km) at a wavelength of 1415 nm. In addition, based on simulation analysis, the lowest negative dispersion variation is achieved in the C-band for DC-PCF with the following parameters: $d_1=0.8$ μm, $d_2=0.45$ μm, $d_3=1.35$ μm and $\Lambda=1.5$ μm. It has ultra-flattened negative dispersion with slope=0.01142 (ps/nm^2/km) over the C-band.

As simply indicated in the previous section, the inner core structure has the dominant effect on dispersion characteristic. As a result, dispersion is more sensitive to the inner hole diameter, d_1, which plays important role in the inner core structure (see Fig. 11).

Also, d_2 is the crucial parameter of the DC-PCF to achieve negative dispersion over a wide wavelength range (see Fig. 12). It is mainly related to the fact that d_2 has the most important role in forming the second core. The DC-PCF with d_2 lower and higher than 0.45 μm cannot have relatively high negative dispersion over the E-band to the U-band.

It can be inferred from Fig. 13, that since rings with air-hole diameters of d_3 are farther from the central core, it has no considerable effect on dispersion in comparison with d_1.

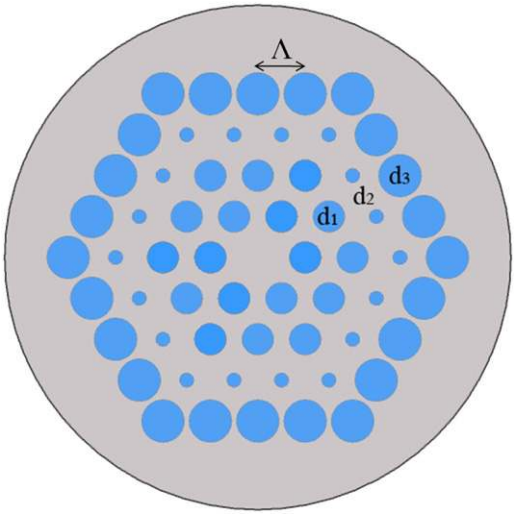

Fig. 18. Cross-sectional view of the DC-PCF with the ring–core at the third ring.

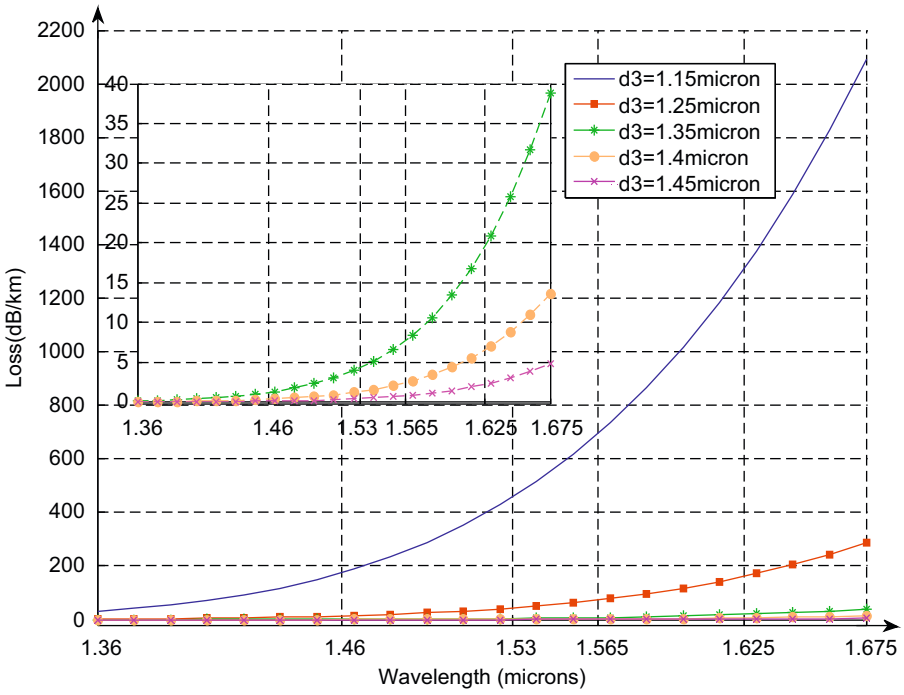

Fig. 17. Loss curve of the DC-PCF as a function of wavelength with different d_3. $d_1=1$ μm, $d_2=0.45$ μm and $\Lambda=1.5$ μm.

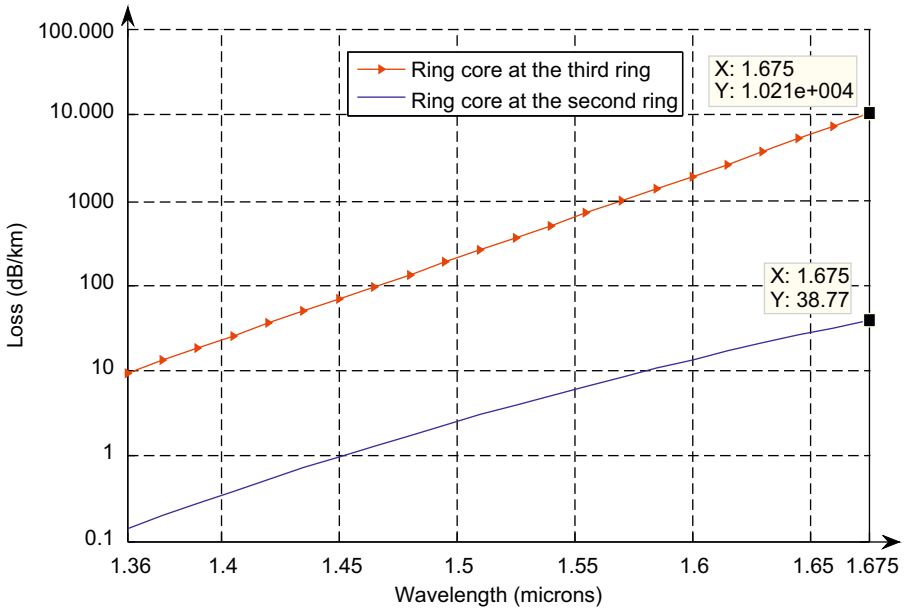

Fig. 19. Loss curves of the DC-PCF as a function of wavelength, with different ring-core location. $d_1 = 1$ μm, $d_2 = 0.45$ μm, $d_3 = 1.35$ μm and $\Lambda = 1.5$ μm.

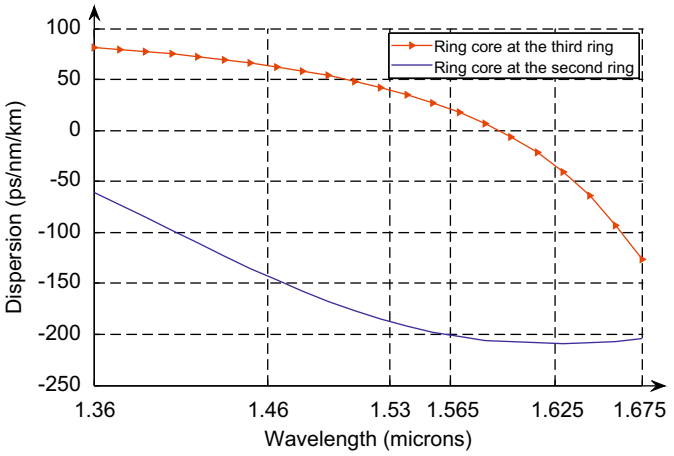

Fig. 20. Dispersion curves of the DC-PCF as a function of wavelength, with different ring-core location. $d_1 = 1$ μm, $d_2 = 0.45$ μm, $d_3 = 1.35$ μm and $\Lambda = 1.5$ μm.

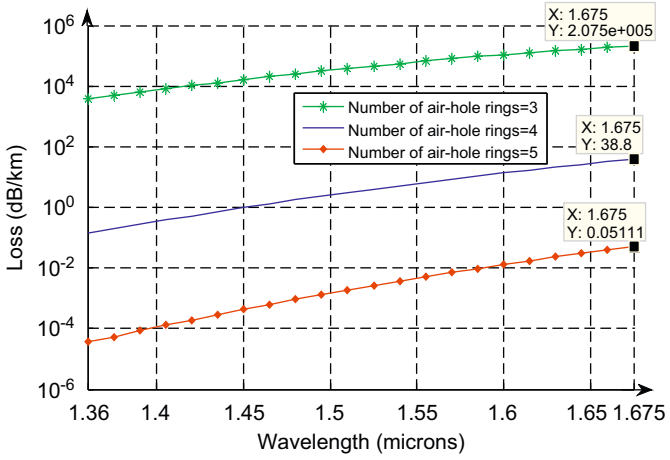

Fig. 21. Loss curves of the DC-PCF as a function of wavelength, with different number of air-hole rings. $d_1 = 1$ μm, $d_2 = 0.45$ μm, $d_3 = 1.35$ μm and $\Lambda = 1.5$ μm

The loss characteristics of DC-PCF with $d_1 = 1$ μm, $d_2 = 0.45$ μm, $d_3 = 1.35$ μm and $\Lambda = 1.5$ μm within the wavelength range of 1360–1675 nm are shown in Fig. 14. With respect to Fig. 14, the loss of the designed DC-PCF is 0.1–1.25 (dB/km) over the E-band. In addition, the DC-PCF shows the losses of 1.25–4.5 (dB/km), 4.5–8.05 (dB/km), 8.05–19.72 (dB/km) and 19.72–38.77 over S, C, L and U bands, respectively.

Figs. 15–17 illustrate the loss of the DC-PCF with altering the hole diameters: d_1, d_2 and d_3, respectively. As Fig. 15 shows, the loss increases with increase in the hole diameter of the inner ring: d_1. It is due to the decrease of the effective core area with increase in d_1.

According to Fig. 16, the loss increases with increase in d_2 firstly, and then it decreases. In this case, there are two mechanisms: ring core role and air filling fraction parameter. On one hand, increase of d_2 degrades the role of ring core, which results in increase of losses. On the other hand, increase of d_2 increases air filling fraction parameter (see (10)), which decreases losses [19]. So, depending on which parameter is dominant, losses increase or decrease. Analysis shows that when d_2 is lower than 0.45 μm, ring core role is dominant, and when d_2 is higher than 0.45 μm, air filling fraction becomes dominant.

The air filling fraction parameter is calculated by the following equation in triangular lattice:

$$F = \frac{\pi}{2\sqrt{3}}\left(\frac{d}{\Lambda}\right)^2 \tag{10}$$

Based on Fig. 17, the loss decreases with increase in d_3. It can be explained by the air filling fraction parameter. With respect to (10), increase of d_3 results in the increase of the air filling fraction, and consequently the decrease of the loss [20].

In the following, the influence of the location of ring-core on dispersion and loss characteristics is studied. Fig. 18 demonstrates cross-sectional view of the DC-PCF with ring-core at the third ring. As shown in Fig. 19, the DC-PCF with ring-core at the third ring has much higher loss. Moreover, Fig. 20 shows that the DC-PCF with ring-core at the second ring has negative dispersion in a wider range of wavelength. It is deduced that the DC-PCF with ring-core at the second ring has higher negative dispersion and lower loss characteristics.

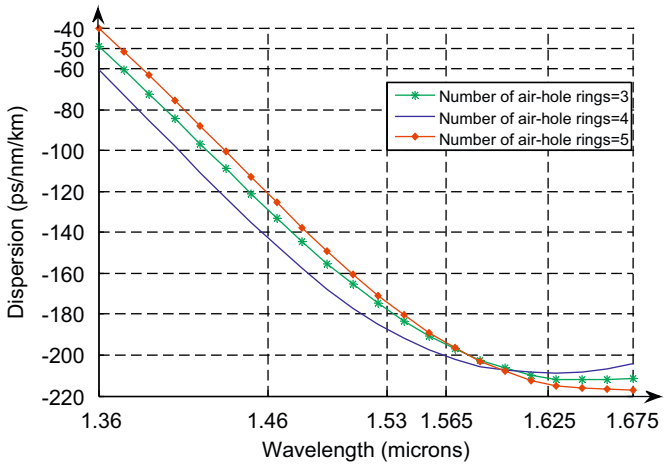

Fig. 22. Dispersion curves of the DC-PCF as a function of wavelength, with different number of air-hole rings. $d_1=1$ μm, $d_2=0.45$ μm, $d_3=1.35$ μm and $\Lambda=1.5$ μm.

Figs. 21 and 22 demonstrate loss and dispersion curves of the DC-PCF with different air-hole rings. As expected, the larger number of air-hole rings provides a more confined guided mode and results in lower confinement loss. Moreover, Fig. 18 shows that negligible loss of 0.46357×10^{-2} (dB/km) at a wavelength of 1550 nm with five air-hole rings can be obtained. It should be noted that more than 20 rings of air-holes usually are required in the cladding region to achieve such a low loss, which has its own fabrication difficulties [19,21].

As it can be seen from Fig. 22, more or less than four air-hole rings lead to decrement of negative dispersion. In the case of five air-hole rings, since the decrease of negative dispersion is not significant, decrease of loss is more valuable. Furthermore, our studies show that using more than five air-hole ring does not result in a negative dispersion in wide range of wavelength, in spite of producing ultra-low loss.

6. Conclusions

In this paper, a DC-PCF for dispersion compensation is proposed. The designed DC-PCF offers relatively high negative dispersion over a wide wavelength range (E, S, C, L and U bands) whereas the recent dispersion compensation designs provide negative dispersion in a single band. It shows the dispersion of -208.8 to -61.5 (ps/nm/km) within the wavelength range of 1360–1675 nm along with the low loss. In addition, the effect of the ring core location is considered. It is found that the DC-PCF with the ring core at the second ring has higher negative dispersion and lower loss in comparison with DC-PCF with the ring core at the third ring. The influence of using more air-hole rings on the DC-PCF characteristics is also investigated. It is understood that ultra low loss of 0.46357×10^{-2} (dB/km) at a wavelength of 1550 nm can be obtained with five air-hole rings. Taking all things into account based on this paper results, appropriate geometric parameters can be chosen for the DC-PCF to achieve the desirable dispersion compensation over different communication bands. Additionally, it is believed that the proposed DC-PCF will have a promising future in ultra-broadband and high-bit-rate transmissions.

References

[1] Fukuchi K, Kasamatsu T, Morie M, Ohhira R, Ito T, Sekiya K, et al., 10.92-Tb/s (273×40-Gb/s) triple-band/ ultra-dense WDM optical-repeatered transmission experiment, In: Proceedings of OFC, Anaheim, CA, 2001 pp. PD24-1–PD24-3.
[2] Nakazawa M, Yamamoto T, Tamura K. Ultrahigh-speed OTDM transmission beyond 1 tera bit-per-second using a femtosecond pulse train. IEICE Transactions on Electronics 2002;E85-C(1):117–25.
[3] Grüner-Nielsen L, Wandel M, Kristensen P, Jorgensen C, Jorgensen L, Edvold B. Dispersion-compensating fibers. Lightwave Technology 2005;23(11):3566.
[4] Russell P. photonic crystal fibers,. Journal of Light Wave Technology 2006;24(12).
[5] Wang J, Jiang C, Hua W, Gao M. Modified design of photonic crystal fibers with flattened dispersion. Optics and Laser Technology 2006;38:169–72.
[6] Hoo YL, Jin W, Ju J, Ho HL, Wang DN. Design of photonic crystal fibers with ultra-low, ultra-flattened chromatic dispersion. Optics Communications 2004;242:327–32.
[7] Gruner-Nielsen L, Knudsen S, Veng T, Edvold B, Larsen C. Design and manufacture of dispersion compensating fiber for simultaneous compensation of dispersion and dispersion slope. In: Proceedings of OFC, San Diego, CA, March 1999 p. 232–4.
[8] Varshney K, Saitoh K, Koshiba M. Novel design for dispersion compensating photonic crystal fiber raman amplifier. IEEE Photonics Technology Letters 2005;17(10).
[9] Nielsen L, Qian Y, Palsottir B, Gaarde P, Dyrbol S, Beng T. Module for simultaneous C+L-band dispersion compensation and Raman amplification. In: Proceeding of OFC, Anaheim, CA, March 2002 p. 65–6.
[10] Lusse P, Stuwe P, Schule J, Unger HG. Stability properties of 3-D vectorial and semivectorial BPMs utilizing a multi-grid equation solver. IEEE Journal of Lightwave Technology 1994;12:487–94.
[11] Li L, Mao J. An improved compact 2-D finite-difference frequency-domain method for guided wave structures. IEEE Microwave and Wireless Components Letters 2003;13:520–2.
[12] Zhu Z, Brown T. Analysis of the fundamental space-filling mode of photonic crystal fibres: a symmetry point of view. Optic Express 2002;10:853–64.
[13] Zho Z, Brown T. Full-vectorial finite-difference analysis of microstructure optical fibers. Optic Express 2002;10:853–64.
[14] Guo S, Wu F, Albin S, Rogowski RS. Photonic band gap analysis using finite-difference frequency-domain method. Optic Express 2004;12:1741–6.
[15] Shen LP, Huang WP, Jian SS. Design of photonic crystal fibers for dispersion-related applications. Journal of Lightwave Technology 2003;21(7):1644–51.
[16] Koshiba M. Full vector analysis of photonic crystal fibers using the finite element method. IEICE Electron 2002;E85-C(4):881–8.
[17] Saitoh K, Koshiba M. Numerical modeling of photonic crystal fibers. Lightwave Technology 2005;23(11):3580–90.
[18] Aliramezani M, Mohammad nejad Sh, Pourmahyabadi M. Design and simulation of a dual-core photonic crystal fiber for dispersion compensation over E to L wavelength band. In: Proceeding on international symposium on telecommunications, August 2008. p. 138–43.
[19] Poli F, Cucinotta A, Selleri S. Photonic Crystal Fibers: Properties and Applications. Springer; 2007 p. 7–52 [chapter 1].
[20] Aliramezani M, Mohammad Nejad S, Pourmahyabadi M, Design of photonic crystal fiber with improved dispersion and confinement loss over all telecommunication bands In: Proceedings on the symposium on high capacity optical networks and enabling technologies, 2008, 141–145.
[21] Wu TL, Chao CH. A novel ultraflattened dispersion photonic crystal fiber. IEEE Photonic Technology Letters 2005;17(1):67–9.